Vietnam Journal of Science and Technology ***63*** *(2) (2025) 347-363*

doi:10.15625/2525-2518/19061

$ZnCo_2O_4$ nanosheets as an efficient electrochemical sensing platform for determination of paracetamol

Nguyen Ngoc Huyen[1, *], Ngo Xuan Dinh[1], Vu Ngoc Phan[1, 2], Le Minh Tung[3, *], Pham Duc Thang[4], Anh-Tuan Le[1, 5, *]

[1]*Phenikaa University Nano Institute (PHENA), PHENIKAA University, Nguyen Van Trac, Yen Nghia, Ha Dong, Ha Noi, Viet Nam*

[2]*Falcuty of Biotechnology, Chemistry and Environmental Engineering, PHENIKAA University, Nguyen Van Trac, Yen Nghia, Ha Dong, Ha Noi, Viet Nam*

[3]*Falcuty of Education and Basic Sciences, Tien Giang University, 119 Ap Bac, Ward 5, My Tho, Tien Giang, Viet Nam*

[4]*Falcuty of Physics, VNU Hanoi University of Science, Vietnam National University, Nguyen Trai, Thanh Xuan, Ha Noi, Viet Nam*

[5]*Falcuty of Materials Science and Engineering, PHENIKAA University, Nguyen Van Trac, Yen Nghia, Ha Dong, Ha Noi, Viet Nam*

[*]Emails: huyen.nguyenngoc@phenikaa-uni.edu.vn, leminhtung@tgu.edu.vn, tuan.leanh@phenikaa-uni.edu.vn

Received: 3 October 2023; Accepted for publication: 29 December 2024

Abstract. $ZnCo_2O_4$ nanosheets (ZCO) were synthesized by a simple method using microwave-assisted hydrothermal technique. X-ray diffraction (XRD), energy-dispersive X-ray spectroscopy (EDX), UV-vis spectroscopy (UV-vis), and scanning electron microscope (SEM) methods were used to study the structural characteristics, morphologies, and sizes of the synthesized materials. A $ZnCo_2O_4$ nanosheet-modified screen-printed electrode (ZCO/SPE) acted as an effective electrochemical sensor for determining paracetamol (PCM). The PCM oxidation peak current response for ZCO/SPE was 37.7 percent higher than that for the bare SPE. Under optimized conditions, the $ZnCo_2O_4$-based electrochemical sensor exhibited a linear response from 0.5 to 100 µM with a high electrochemical sensitivity of 4.27 µA $\mu M^{-1}cm^{-2}$ and a limit of detection (LOD) of 0.19 µM. In addition, the as-synthesized electrochemical sensors had high anti-interference ability and excellent stability for the determination of PCM.

Keywords: $ZnCo_2O_4$, paracetamol, electrochemical sensor.

Classification numbers: 2.5.2

1. INTRODUCTION

Paracetamol (also known as acetaminophen) is a non-steroidal anti-inflammatory drug and is a common medication for its strong antipyretic and analgesic action. It is an over-the-counter (OTC) medicine and popularly used for patients with arthritis, neuralgia, backache, headache, migraines, postoperative pain, etc. [1, 2]. Usually, PCM does not display any negative side effects, but its overdose consumption causes damage to the kidney and liver. In cases of acute

overdose, PCM can also lead to severe and sometimes fatal hepatotoxicity and nephrotoxicity [3, 4]. Thus, establishing one of the simplified and sensitive methods to determine the amount of PCM would be of high importance. The techniques used for the detection of PCM are titrimetric [5], high-performance liquid chromatography [6], spectroscopy [7], opto-chemical and electrochemical sensors [8-10]. Among these methods, the electrochemical sensing method has been regarded as a useful tool for rapid, simple, and sensitive detection [11]. Nevertheless, the limitation of this method in its applicability is the use of pure electrodes (or commercial electrodes) with low electrochemical performance, short-term stability, and slow kinetics of electrochemical reactions on the electrode surface. To overcome these challenges, modifying the working electrode surface is the key research direction pursued. Up to now, most researchers are concentrating on nanomaterials as potential modifiers. The materials usually used in this regard are metal oxides, metals, different carbon nanostructures, and conducting polymers [12]. Currently, metal spinel oxides are one of the most favorite materials for constructing electrochemical sensors because of their chemical and thermal stability, superior redox properties, and cost-effectiveness [13, 14]. Especially, spinel cobaltites have different oxidation states, are easy to synthesize, are low toxic, display high durability in alkaline electrolytes, and have a reasonable price [15, 16]. Among these spinel cobaltites, $ZnCo_2O_4$ has emerged as a highly competent material for many applications in fields such as supercapacitor [17], photocatalysis [18], biosensors and electrochemical sensors [19 - 21] due to its outstanding properties such as relatively low cost, eco-friendly nature, multiple valence states (Co^{2+} and Co^{3+}), superior redox properties, chemical stability, and morphological diversity that includes nanosized rod, porous, sheet, and wire structures. For example, Jiangjiang Zhang *et al*. [22] used $ZnCo_2O_4$ nanosheets synthesized by a hydrothermal method for the detection of p-nitrophenol (PNP) and o-nitrophenol (ONP). Shilin Liu *et al*. [23] reported a non-enzyme glucose sensor based on $ZnCo_2O_4$ micorods by a hydrothermal method. However, the morphological properties and electronic structure of $ZnCo_2O_4$ nanomatrials have decisive effects on the analytical performance of electrochemical sensors. The design of rational nanostructures toward a given analyte has been considered a key to enhancing the analytical performance of $ZnCo_2O_4$-based electrochemical sensors. Thus, further efforts are still required in novel $ZnCo_2O_4$ nanostructure designs for high-performance electrochemical sensors.

In this work, a simple method using microwave-assisted hydrothermal technique is developed to synthesize two-dimensional spinel nanosheets comprising $ZnCo_2O_4$ nanoparticles. The $ZnCo_2O_4$ nanosheets showed an excellent electrocatalytic oxidation capability towards PCM with a marked decrease in the overvoltage and an increase of oxidation current response. The $ZnCo_2O_4$ nanosheets-based electrochemical sensor showed wide dynamic linear ranges, low limit of detection, great sensitivity, and good repeatability. The practical applicability of the sensor was also investigated by sensing the PCM in pharmaceutical samples.

2. EXPERIMENTAL SECTION

2.1. Materials

Zinc nitrate hexahydrate ($Zn(NO_3)_2.6H_2O$, 99 %), Cobalt (II) nitrate hexahydrate ($Co(NO_3)_2.6H_2O$, 98.5 %), and Urea ($(NH_2)_2CO$, 99 %) were manufactured by Xilong Scientific Co., Ltd. (Guang-dong, China). Paracetamol (PCM, 99 %) was purchased from the National Institute of Drug Quality Control (Ha Noi, Viet Nam). A phosphate-buffered saline (PBS) solution (0.1 M, pH 7.3) was prepared using KCl (> 99.5 %) and KH_2PO_4 (> 99.5 %) provided by Merck KgaA, Germany); $Na_2HPO_4.12H_2O$ (> 99 %) was purchased from Guanghua

Chemical Factory Co. Ltd., China. $K_3[Fe(CN)_6]$ (> 99.5 %), $K_4[Fe(CN)_6]$ (> 99.5 %), and NaCl (> 99.5 %) were acquired from Xilong Scientific Co. Ltd., China. The pH value of the PBS buffer solution was regulated by H_3PO_4 (> 85 %), and NaOH (> 96 %) which are products of Duc Giang Chemical JSC, Viet Nam. All the chemicals were used in their original form (without any additional purification). Carbon screen-printed electrodes (SPE) were bought from Metrohm Vietnam Co., Ltd.

2.2. Synthesis of $ZnCo_2O_4$ nanosheets (ZCO)

$ZnCo_2O_4$ nanosheet samples were prepared by a microwave-assisted hydrothermal method. Initially, 0.48 g of $Co(NO_3)_2.6H_2O$ and 0.446 g of $Zn(NO_3)_2.6H_2O$ were dissolved in 250 mL of double-distilled water. The mixture was magnetically stirred for 15 minutes at 25 ℃. After that, 60 mM Urea solution was slowly added to the above solution. Next, the mixture was put into an autoclave and heated for 30 minutes at 140 °C. At the end of the reaction time, the autoclave was naturally cooled to under 30 °C. Then, the precipitation was washed several times by double-distilled water and dried at 80 °C for 12 hours. $ZnCo_2O_4$ powder was obtained after being calcined at 400 °C.

2.3. Preparation of modified electrode and real samples

A dropping technique was used to prepare the modified electrode. Initially, the bare SPE was cleaned with ethanol and double-distilled water, and then allowed to dry at room temperature. Next, 3 mg of ZCO sample was dispersed into double-distilled water (concentration 1 mg/mL) and sonicated for 1 hour to achieve a stable suspension. Then, 8 µL of the $ZnCo_2O_4$ solution was dropped onto the working electrode. After drying for 3 hours at 40° C in air, the electrode was ready to use.

Panadol tablets (500 mg paracetamol) and Hapacol powder (80 mg paracetamol) were the two types of medications we used in this investigation. Firstly, 600 mg of Panadol tablets was finely powdered in an agate mortar. Next, each powder was dissolved in double-distilled water by a vortex mixer to get the desired concentration (10, 30, 50 µM) and then used for pharmaceutical sample studies.

2.4. Materials characterization

The crystalline structure of the ZCO sample was studied by a Bruker D5005 X-ray Diffractometer using CuK_α radiation (λ = 0.154056 nm). Fourier transform infrared spectroscopy (FTIR) spectra were investigated using an IRAffinity-1S spectrometer in the range from 200 cm^{-1} to 4000 cm^{-1}. The morphology of the $ZnCo_2O_4$ sample was recorded by a scanning electron microscopy (SEM) system. The energy-dispersive spectroscopy (EDS) mapping was applied to characterize the element distribution (HORIBA model 7593-H, attached on FESEM HITACHI S-4800). The UV-vis absorbance spectra were examined (HP 8453 spectrophotometer), and the pH measurements were carried out using an IC-PH60 pH tester kit, America.

2.5. Electrochemical measurements

The electrochemical properties and electrochemical performance of the electrodes in this study were evaluated using a Palmsens4 electrochemical workstation (Netherlands) at temperatures ranging from 25 to 27 °C. Initially, electrochemical measurements, including electrochemical impedance spectroscopy (EIS) and cyclic voltammetry (CV) were performed by

applying a potential from -0.3 V to 0.6 V in 0.1 M KCl solution containing 5 mM $K_3[Fe(CN)_6]/K_4[Fe(CN)_6]$ at a scan rate from 0.05 V s^{-1}. EIS measurements were carried out at a potential of −0.2 V in the frequency range from 0.01 to 50 KHz. Next, the electrochemical performance of PCM on the modified electrodes was investigated using CV and differential pulse voltammetry (DPV) techniques in a 0.1 M PBS buffer solution. DPV measurements were performed under the following conditions: E_{pluse} = 0.075 V, T_{pulse} = 0.25 s, scan rate of 0.006 V s^{-1}. CV measurements were carried out at scan rates from 0.01 to 0.06 V s^{-1} over a potential range between 0.0 and 0.8 V.

3. RESULTS AND DISCUSSION

3.1. Characterization of $ZnCo_2O_4$ nanosheets

To investigate the phase and purity of the materials, XRD diffraction was recorded in the 2θ range of 10° - 70° as depicted in Figure 1a.

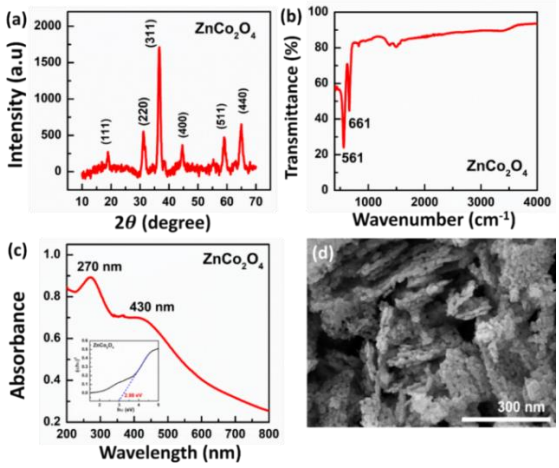

Figure 1. (a) XRD patterns, (b) FTIR spectrum, (c) UV-Vis absorption spectrum, Tauc plot (inset), and (d) SEM image of the synthesized materials $ZnCo_2O_4$.

In particular, the peaks centered at 2θ of 18.85°, 31.15°, 36.62°, 44.60°, 59.08°, and 64.93° were indexed to the (111), (220), (311), (400), (511), and (440) diffraction planes of the standard pattern for $ZnCo_2O_4$ (JCPDS No. 23-1390), respectively [24]. There are no other diffraction peaks on the XRD spectra, indicating that the synthesized product is pure spinel with good crystal structure. The Debye-Scherrer formula is applied to calculate the crystal size of $ZnCo_2O_4$ nanomaterials. The average crystallite size of $ZnCo_2O_4$ is approximately 18.6 nm. Additionally, the crystal plane spacing calculated according to Bragg's law using the (311) plane is 0.245 nm, which agrees well with the value previously reported for the (311) plane of the $ZnCo_2O_4$ spinel phase [25]. Furthermore, the spacing d between adjacent (hkl) lattice planes for cubic crystal structure of spinel oxide is given by $a = d_{(hkl)}\sqrt{(h^2 + k^2 + l^2)}$, where a is crystal lattice paremeters. Consequently, a is determined to be about 8.12 A˚. FT-IR spectroscopy is an absorptive technique used to identify the presence of various functional groups in a complex molecule. Figure 1b shows two absorption bands at 561 cm^{-1} and 661 cm^{-1}, indicating stretching vibration of Co-O and Zn-O bonds in the crystal lattice of $ZnCo_2O_4$ [26]. The evidence from the

obtained FTIR spectrum further demonstrated the formation of $ZnCo_2O_4$ through exhibiting its metal oxide vibrations in the fingerprint region.

The optical property of $ZnCo_2O_4$ nanosheets is investigated using a UV-Vis spectrophotometer. Figure 1c presents the UV-vis absorption spectra of $ZnCo_2O_4$. It can be observed that $ZnCo_2O_4$ possesses strong absorption in both the visible light range (absorption peak at 430 nm) and ultraviolet light range (absorption peak at 270 nm). Furthermore, the optical band gap energy (E_g) of $ZnCo_2O_4$ can be estimated from Tauc's plot according to the equation:

$$\alpha h\upsilon = K(h\upsilon - E_g)^n$$

where α is the absorption coefficient, $h\upsilon$ is the photon energy in eV, K is the proportionality constant, n = ½ and 2 for direct and indirect transition, respectively. As shown in the inset in Figure 1c, the band gap value of $ZnCo_2O_4$ was calculated to be 2.98 eV. The E_g value of ZCO in this work was very close to that in previous reports [27, 28].

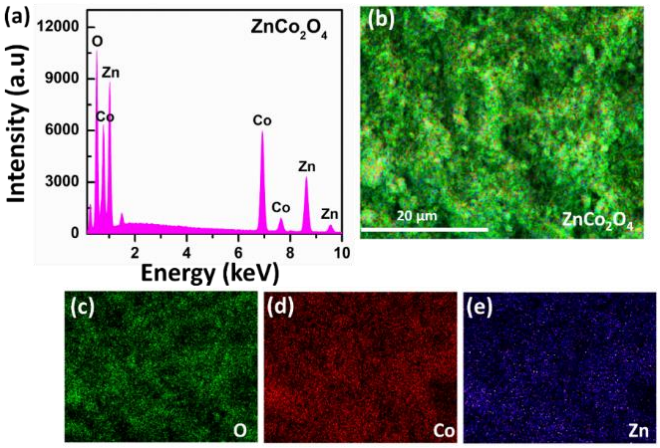

Figure 2. (a) EDS spectra, (b) EDS element mapping of $ZnCo_2O_4$ nanomaterial, and (c-e) elemental mapping of the elements O, Co, and Zn. The scale bar in c-e is 20 µm.

The morphologic characterization of $ZnCo_2O_4$ samples was examined via SEM images as depicted in Figure 1d. The overall morphology of $ZnCo_2O_4$ looks like nanosheet arrays with a length of 100 to 150 nm. In addition, the nanosheets' surface seems coarse and shows a surface structure that is relatively porous. The SEM image also clearly displayed that the porous nanosheets were composed of many regular nanoparticles with a diameter of about 20 nm (this is consistent with the XRD result). The thickness of the nanosheets was calculated to be around 15 nm. Besides, the EDS technique and the EDS elemental mapping in Figure 2 further confirmed the presence and homogeneous distribution of Zn, Co, and O elements in the $ZnCo_2O_4$ nanosheet, with oxygen content of ~ 35.82 wt.%, zinc content of ~ 34.19 wt. %, and cobalt content ~ 29.99 wt.%.

3.2. Electrochemical characteristics of $ZnCo_2O_4$/SPE

The electrochemical properties of both pure SPE and ZCO/SPE were studied by CV measurements in 0.1 M KCl containing 5 mM $[Fe(CN)_6]^{3-/4-}$ as redox probes (as depicted in Figure 3).

As can be seen, a pair of well-defined redox peaks of Fe^{2+}/Fe^{3+} was observed on both two electrodes at a scan rate of 50 mV s^{-1}. Nevertheless, the obvious difference was pointed out from

the redox peak currents. For pure SPE, it displayed an anodic current value of 166.7 µA. Meanwhile, for ZCO/SPE, this value was found to be about 237.3 µA. The differences in conductivity, electron-transfer efficiency, and the inherent special features of $ZnCo_2O_4$ nanosheet in the redox process could be responsible for the variations in the redox peak current of the ZCO/SPE modified electrode. In addition, ZCO in the shape of nanosheet can significantly improve surface area of SPE electrode, providing more active sites for redox reactions. The electroactive surface area (EASA) of SPE and ZCO/SPE was investigated using CV measurements. These measurements were performed at scan rates from 10 mV s^{-1} to 60 mV s^{-1} under the same conditions (Figure 4).

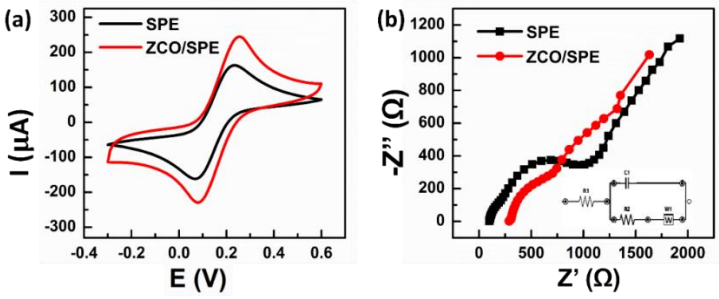

Figure 3. CV curves (a) and EIS (b) of pure SPE and ZCO/SPE were recorded in 0.1 M KCl solution containing 5 mM $Fe(CN)_6^{3-/4-}$.

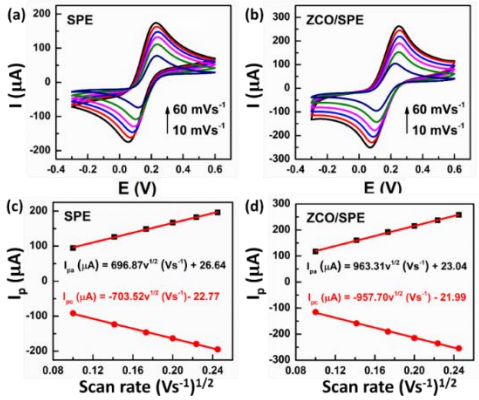

Figure 4. (a–b) CV profiles of the bare SPE and ZCO/SPE at different scan rates (10 mV s^{-1}–60 mV s^{-1}); and (c–d) the linear plots of the square root of the scan rate and the redox peak current signal. All measurements were performed in 0.1 M KCl solution containing 5 mM $[Fe(CN)_6]^{3-/4-}$.

The EASA value was calculated by the Randles-Sevcik equation as follows [29, 30]:

$$I_p = 2.69 \times 10^5 n^{3/2} D^{1/2} A C v^{1/2}$$

where D is diffusion coefficient of $[Fe(CN)_6]^{3-/4-}$ (6.5×10^{-6} cm^2 s^{-1}), n = 1 (number of electrons participating in the redox reaction), v is the scan rate, C is the concentration of $[Fe(CN)_6]^{3-/4-}$, and A is the electroactive surface area. As shown in Figures 4a, 4b, when the scan rate increased from 10 mV s^{-1} to 60 mV s^{-1}, the redox current intensity also increased in a linear relationship. From that, the EASA values for the ZCO/SPE and pure SPE could be calculated from the slope of the plots of peak currents with square root of the scan rate (Figures 4c, 4d). The EASA of the electrodes was acquired as 0.057 cm^2 and 0.113 cm^2 for bare SPE and ZCO/SPE, respectively. Obviously, the modification by the $ZnCo_2O_4$ nanosheet provided a better current response, larger

active surface area, and more effective electrochemical performance than the pure SPE. This outcome is in line with electrochemical impedance spectroscopy (EIS) results recorded at the changed and unchanged electrodes. Figure 3b displays the Nyquist plots obtained over the frequency range from 0.01 Hz to 50 kHz in 0.1 M KCl containing 5 mM $[Fe(CN)_6]^{3-/4-}$. In a Nyquist plot, R_{ct} corresponds to the circumference of a semicircle in the higher frequency region. A linear region in the lower frequency corresponds to mixed kinetic-control and diffusion-control processes [31]. As can be seen in Figure 3b, the bare SPE electrode exhibited a larger semicircle than that of ZCO/SPE. Indeed, the R_{ct} values were estimated to be about 643.4 Ω, and 322.4 Ω for bare SPE, and ZCO/SPE, respectively. It is evident that as compared to the bare SPE, the ZCO-based modified electrode had a lower electron transfer resistance. It implies that the $ZnCo_2O_4$ nanosheets on the surface of SPE could boost electron transfer rate and reduce charge transfer resistance, resulting in an increase in conductivity. The obtained results indicate that the $ZnCo_2O_4$ nanosheet-based electrode exhibits superior electrochemical characteristics compared to commercial SPE.

3.3. Electrochemical behaviors of paracetamol

The electrochemical behavior of PCM at unmodified and modified electrodes was evaluated using CV measurements at a scan rate of 50 mV s^{-1} in 0.1 M PBS buffer solution (pH 7.3). The CV measurements were traced in the presence and absence of PCM molecules at all electrodes. As shown in Figure 5a, there were no redox peaks in the PBS solution, and when PCM was added to the PBS buffer solution, a pair of redox peaks characteristic of PCM molecules appeared within the potential range of 0.2 - 0.5 V [32 - 34]. The obtained anode peaks were sharper than the cathode peaks on both SPE and ZCO/SPE electrodes. Therefore, in this work, we focus on the change of anode peaks. For the ZCO/SPE modified electrode, the observed sharp anode peak demonstrated an oxidation process of PCM at a potential of 0.35 V; meanwhile, this peak can be observed at a higher positive potential of 0.37 V for the unmodified electrode, indicating a high electrocatalytic activity of $ZnCo_2O_4$ for the oxidation process of PCM. In addition, the ZCO/SPE electrode also displayed a higher oxidation current response of PCM, and a lower background current in comparison with pure-SPE electrode. Indeed, the oxidation peak current of PCM at the ZCO/SPE modified electrode (19.32 μA) was about 1.4-fold larger as compared to the unmodified electrode (14.03 μA), respectively. The results indicated that the $ZnCo_2O_4$ nanosheets play a role as an efficient electrocatalyst for the oxidation reaction of PCM.

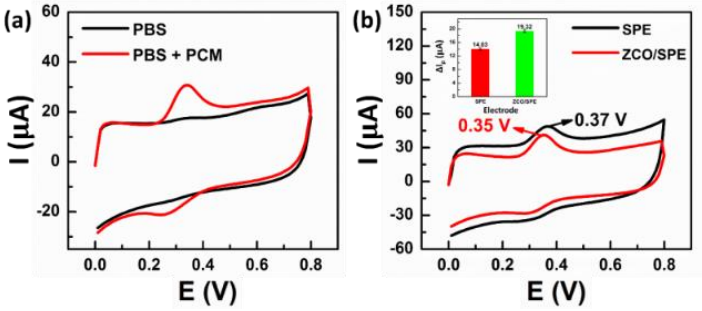

Figure 5. (a) CV recorded on pure SPE in PBS buffer solution (pH 7.3) in the presence and absence of PCM analyte and (b) CV curves of bare SPE and ZCO/SPE. Inset: plot of comparing peak currents between the unmodified and modified electrodes.

3.4. The effect of pH and scan rate

The effect of pH and scan rate on the redox response of PCM were investigated by DPV and CV measurements. The CV measurements with various scan rates from 10 to 60 mV s^{-1} were carried out in 0.1 M PBS solution (pH 7.3) containing 100 µM PCM, as shown in Figure 6a. As seen from the CV curves, the oxidation peak current of PCM rose linearly as the scan rate increased from 10 mV s^{-1} to 60 mV s^{-1}, corresponding to the linear regression equation of I_{pa} (µA) = 0.292ν (mVs^{-1}) + 0.027 (R^2 = 0.99) (Figure 6b). It could be emphasized that the electrochemical redox reaction of PCM occurred in the surface adsorption-controlled process on ZCO/SPE. Furthermore, when the scan rate increased, the oxidation peak potential position changed marginally toward the positive potential side. The linear relationship between the oxidation peak potential (E_p) and the scan rate (ν) and the natural logarithm of the scan rate (ln (ν)) was displayed in the regression equations E_{pa} = 1.3ν (V s^{-1}) + 0.275 (R^2 = 0.93) and E_{pa} = 0.037 ν (V s^{-1}) + 0.451 (R^2 = 0.97), respectively (Figures 6c, 6d). Based on the Laviron equation [35, 36]:

$$E_{pa} = E_o + (\frac{RT}{(1-\alpha)nF})\ln(\frac{(1-\alpha)nF}{RTK_{et}}) + (\frac{RT}{(1-\alpha)nF})\ln\nu$$

where the slope of the linear lines is RT/(1-α)nF with F = 96500 C mol^{-1}, α is the electron transfer coefficient, R = 8.314 J mol^{-1} K^{-1}, k_{et} is the electron transfer rate constant, T = 298 K, and n is the number of electrons transferred, the (1-α)n value was calculated to be about 0.694. From that, the number of electrons involved in the reaction being two electrons with the charge transfer coefficient (α) was calculated to be 0.653. Besides, the pH value of the PBS solution is one of the factors that greatly affects the electrocatalytic activity of the electrochemical sensor. In this study, the influence of pH value was investigated by DPV measurements at a scan rate of 50 mV s^{-1} in a mixture containing of PCM (100 µM) with various pH values from 3.0 to 11.3 (Figure 7).

Scheme 1. Suggested redox mechanisms of paracetamol.

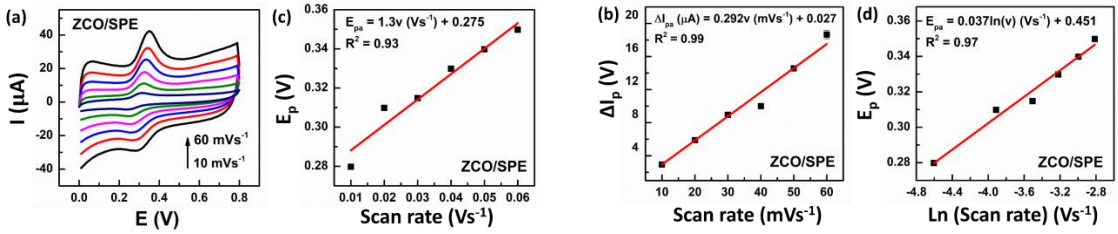

Figure 6. (a) CVs of 100 µM PCM with various scan rates (10, 20, 30, 40, 50, 60 (mV s^{-1})) on ZCO/ SPE in 0.1 M PBS (pH = 7.3), (b) Plot of the dependence of the oxidation peak current on the scan rate, (c) a linear relationship between scan rate and anode peak positive, and (d) Plot of the dependence of E_p on natural logarithm of scan rate [ln(ν)].

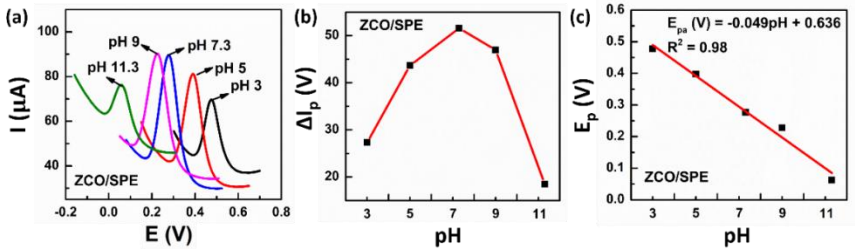

Figure 7. (a) DPV recorded on ZCO/SPE at different pH values of PBS solution (3.0 - 11.3) containing 100 μM PCM, (b) Dependence of oxidation peak current on pH value, (c) Dependence of peak current signal on pH value.

As can be seen, the ZCO/SPE modified electrode displayed changes in both the oxidation peak potential position and current signal. When the pH value of the PBS buffer solution decreased from 11.3 to 3.0, the oxidation peak potential position of PCM moved towards positive potential. The oxidation peak current intensity of PCM reached its maximum at pH 7.3 and then declined gradually. Thus, a suitable pH value of 7.3 was selected to achieve the best sensitivity for the next electrochemical studies. The peak potential position also varied when the pH value of the PBS solution was altered, indicating that protons were involved in the oxidation of PCM. On the other hand, in Figure 7c the relationship between oxidation peak potential positions and pH values is linear with the equation: E_{pa} (V) = -0.049pH + 0.636 (R^2 = 0.98). The slope of the linear line is -0.049 V/pH, which is close to the theoretical value proposed by Nernst (-0.059m/n) V/pH, in which the protons and electrons participating in the PCM's oxidation process are denoted by the letters m and n, respectively. As a result, two protons and two electrons participated in the oxidation process of PCM happening at the electrode surface (due to the n:m value being determined to be around 1.2), corresponding to several previously proposed mechanisms for the electrochemical oxidation of PCM, as presented in Scheme 1. This redox process corresponds to the transformation of PCM to N-acetyl-p-quinone-imine (NAPQI) and vice versa [37].

3.5. Effect of ZCO amount and accumulation time

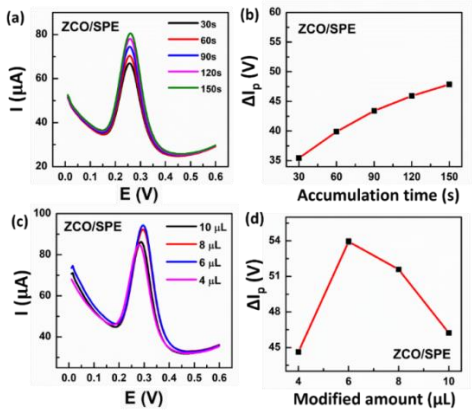

Figure 8. Influence of accumulation time (30 - 150 s) (a, b) and the amount of $ZnCo_2O_4$ nanosheets on SPE electrode (c, d) of ZCO/SPE.

To optimize the experimental conditions, the influence of the amount of $ZnCo_2O_4$

nanosheets and accumulation time on the electrochemical reaction of PCM detection was investigated. The electrochemical measurements to investigate accumulation time were performed by DPV method in 0.1 M PBS buffer solution (pH = 7.3) with a concentration of 100 μM PCM for a period of 30 to 150 s. The obtained results presented in Figures 8a and 8b show that increasing the accumulation time from 30 s to 150 s, a gradual increase in the anode peak current of PCM was observed. However, when the accumulation time was changed from 120 s to 150 s, the error and instability of the measurements also increased. Hence, an accumulation time of 120 seconds was used for further experiments.

The amount of $ZnCo_2O_4$ nanosheets on the modified electrode surface was studied in the range of 4 to 10 μL by monitoring the PCM oxidation current (using DPV method in 0.1 M PBS (pH 7.3) containing 100 μM PCM). The obtained results in Figures 8c and 8d display oxidation peak currents of PCM which increased with increasing the volume of modifier amounts from 4 to 6 μL. Nevertheless, the oxidation peak current gradually decreased when the amount of $ZnCo_2O_4$ nanosheets gradually increased from 6 to 10 μL. Therefore, for the further electrochemical experiments, 6 μL of $ZnCo_2O_4$ (1 mg/mL) was chosen to modify the SPE working electrode surface.

3.6. Determination of paracetamol

In order to evaluate the electrochemical performance of $ZnCo_2O_4$-modified electrode toward PCM, DPV measurements were performed at PCM concentrations between 0.5 and 500 μM. All the DPV measurements at various PCM concentrations on ZCO/SPE were carried out in 0.1 M PBS solution (pH 7.3, accumulation time of 120 s, and ZCO amount of 6 μL). Figure 9 shows the calibration plots and DPV curves of the oxidation peak current intensity against different PCM concentrations. On the modified electrode, it is seen that the oxidation peak currents increased proportionally to the PCM concentration. The oxidation peak current was linear with the PCM concentration in the range of 0.5 - 100 μM for ZCO/SPE, and the obtained linear regression equation was I_{pa} (μA) = 0.482C_{PCM} (μM) + 1.065 (R^2 = 0.99). Furthermore, the limit of detection (LOD) and the electrochemical sensitivity of the electrochemical sensor were determined using the following equations [30]:

$$\text{Sensitivity 2} = a/A$$

$$\text{LOD} = 3.3\ SD/a$$

where A is the electroactive surface area (EASA), a is the slope of the calibration curve, and SD is the standard deviation of a blank sample. So, via the slope value of the obtained linear line, the LOD was calculated to be around 0.19 μM and the electrochemical sensitivity towards PCM was found at 4.27 $\mu A.\mu M^{-1}cm^{-2}$ for ZCO/SPE.

Besides, a comparison of the linear range value and LOD values of ZCO/SPE in this work with previously published studies using different modified electrodes for PCM determination is given in Table 1. As a result, $ZnCo_2O_4$ nanosheet-based modified SPE is superior to other modified electrodes because of its extremely low LOD, broad linear range, and high sensitivity. Based on the electrochemical results obtained, it should be emphasized that $ZnCo_2O_4$-based nanosheets showed promise as an excellent sensing platform for rapid detection of PCM in real samples with the advantages of $ZnCo_2O_4$ nanosheets such as large surface area, high electrical conductivity, and excellent electrochemical stability.

Table 1. PCM detection abilitiy by various electrochemical nanosensors.

No.	Electrode	Method	Linear range (µM)	LOD (µM)	Ref.
1	CNT-P/CPE	SWV	10 – 100	1.1	[38]
2	PANI–MWCNTs/GCE	SWV	1 – 100	0.25	[39]
3	MWCNTs/poly(Gly)/GCE	DPV	0.5 – 10	0.5	[40]
4	f-MWCNTs/GCE	DPV	3 – 300	0.6	[41]
5	$NiCo_2O_4$ nanoplates/1-hexyl-3-methylimidazolium tetrafluoroborate/CPE	DPV	0.004 - 115 µM	1 nM	[42]
6	CuO-$CuFe_2O_4$/CPE	DPV	0.01–1.5	0.007	[43]
7	NiO/GCE	DPV	0.048 - 130	0.23	[44]
8	Ethynylferrocene–NiO/MWCNT/CPE	DPV	0.8 - 600	0.5	[45]
9	$ZnCo_2O_4$ nanosheets)/SPE	DPV	0.5 - 100	0.19	This work

CNT-P: Poly(3-aminophenol) and CNT; CPE: Carbon paste electrode; SWV: Square wave voltammogram; PANI–MWCNTs: Polyaniline–multi-walled carbon nanotubes; GCE: Glassy carbon electrode; MWCNTs/poly(Gly)*: Multi-walled carbon nanotubes/poly(glycine); DPV: Differential pulse voltammetry;* f-MWCNTs*: Acid functionalized multi-wall carbon nanotubes; SPE: Screen-printed electrode.*

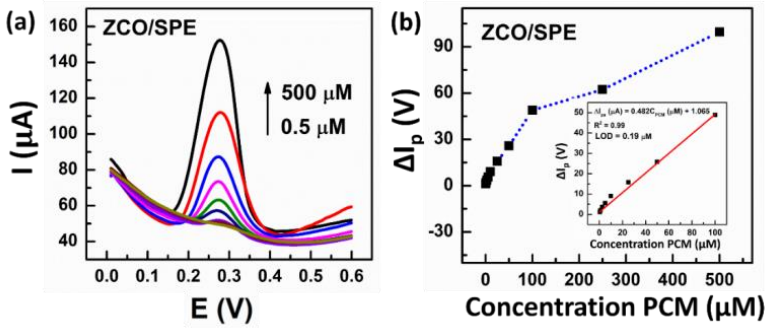

Figure 9. (a) DPV curves of different PCM concentrations, (b) Plots of peak current vs. concentration of PCM. Inset: a linear relationship between peak current intensity and 0.5 - 100 µM PCM concentration with error bars.

3.7. Repeatability, stability, selectivity, and real sample analysis

Investigating the repeatability, stability, and selectivity of the ZCO/SPE modified electrode were conducted in this work. Firstly, to investigate the repeatability, DPV measurements were repeated ten times in 0.1 M PBS (pH = 7.3) containing 100 µM PCM at 50 mV s^{-1}.

The obtained result in Figure 10a points out that ZCO/SPE had outstanding repeatability with a relative standard deviation (RSD) value of 1.02 %. This implied that ZCO/SPE-based

electrochemical sensor shows excellent repeatability. Secondly, for evaluating long-term stability, ZCO/SPE was stored for two weeks under atmospheric conditions and room temperature. Figure 10b displays the DPV measurements performed on the ZCO/SPE electrode in a 0.1 M PBS solution (pH 7.3) with 100 µM PCM at various storage intervals. As expected, after two weeks of storage, the value of the current signal was still around 95 % compared to the initial value.

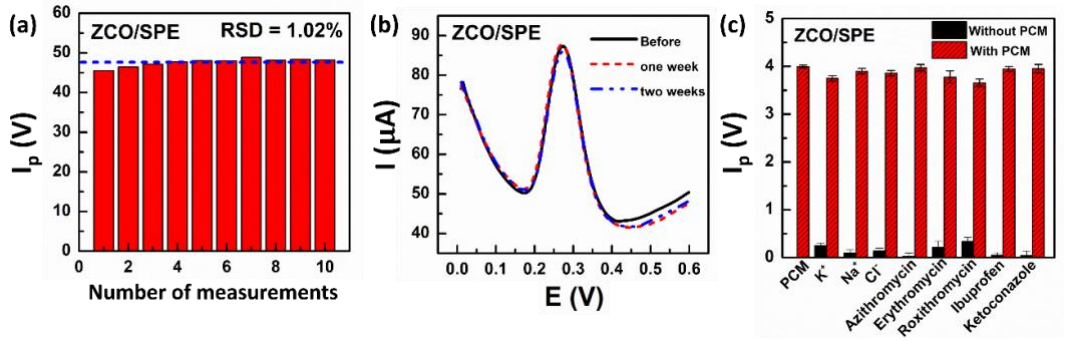

Figure 10. (a) The repeatability, (b) stability, and (c) selectivity of ZCO/SPE.

This exhibited the good stability of the prepared electrode. In order to evaluate the selectivity of the proposed electrochemical sensor in the determination of PCM, the DPV technique was carried out to investigate the influence of several metal ions (such as Na^+, K^+, and Cl^-) and common medicines (azithromycin, erythromycin, roxithromycin, ibuprofen, and ketoconazole) at 20-fold concentrations on the detection of 5 µM PCM (Figure 10c). The obtained results pointed out that no significant influence on the current response of PCM was observed even under high concentrations of interfering substances. This means that the ZCO/SPE modified electrode has good anti-interfering capability for the electrochemical detection of PCM. According to these consequences, the ZCO/SPE-based electrochemical sensor is a potential candidate for real sample analysis with good long-term stability, selectivity, and repeatability.

Table 2. Determination results of PCM in pharmaceutical samples (n = 3).

Sample	Nominal value (µM)	Found (µM)	Recovery (%)	RSD (%)[n]
Hapacol (80 mg)	10	7.08	76.1	5.5
	30	28.12	94.2	3.4
	50	41.15	83.1	1.2
Efferagan (500 mg)	10	9.02	91.9	1.5
	30	27.47	92.1	1.9
	50	42.64	85.9	0.6

To examine the practical application of electrochemical sensors using $ZnCo_2O_4$/SPE-based electrodes in pharmaceutical samples, the concentration of PCM in two kinds of drug samples (1) powder drug (Hapacol 80 mg) and (2) tablet drug (Efferagan 500 mg) was determined. The results of the analysis are presented in Table 2. The ZCO-based electrochemical sensor showed recoveries ranging from 76.1 to 94.2 % with RSD values of 3.2 % or less (n = 3). This result proves that the electrochemical sensor based on $ZnCo_2O_4$ nanosheets has practical applications for determining PCM in powder and tablet drug samples.

4. CONCLUSIONS

In this study, we have reported a simple and rapid technique for the synthesis of $ZnCo_2O_4$ nanosheets via microwave-assisted hydrothermal method. The synthesized $ZnCo_2O_4$ exhibits a single phase, good crystallinity and has a morphology similar to nanosheet arrays with a thickness of about 15 nm. The $ZnCo_2O_4$ nanosheets showed outstanding electrochemical characteristics with a larger electroactive surface area and lower electron transfer resistance compared with pure SPE. Besides, $ZnCo_2O_4$ also exhibited excellent electrocatalytic activity for the redox process of paracetamol, enabling the electrocatalytic detection of PCM at low overpotential. Under optimized conditions, the ZCO-based electrochemical sensor responded linearly to PCM in the range from 0.5 to 100 μM with a low detection limit of 0.19 μM and high electrochemical sensitivity of 4.27 $\mu A.\mu M^{-1}cm^{-2}$. Furthermore, the designed sensor exhibited a good stability, high repeatability, and practical applicability for analyzing pharmaceutical samples with acceptable recoveries. From the results obtained, it is evident that $ZnCo_2O_4$ with its unique 2D structure could be a potential candidate for electrochemical sensing applications in pharmaceutical analysis.

Acknowledgements. This research was supported by the Vietnam National Foundation for Science and Technology Development (NAFOSTED) through a fundamental research project (103.02-2020.68).

CRediT authorship contribution statement. Nguyen Ngoc Huyen: Methodology, Investigation, Writing-Original Draft. Ngo Xuan Dinh: Formal analysis, Validation. Vu Ngoc Phan: Validation, Investigation. Le Minh Tung: Funding acquisition, Conceptualization, Investigation. Pham Duc Thang: Investigation, Visualization. Le Anh Tuan: Conceptualization, Methodology, Supervision, Writing-review and editing.

Declaration of competing interest. The authors declare that they have no known competing financial interests or personal relationships that could have appeared to influence the work reported in this paper.

REFERENCES

1. Hochberg M. C., and Dougados M. - Pharmacological therapy of osteoarthritis, Clin. Rheumatol **15** (4) (2001) 583-593. https://doi.org/10.1053/berh.2001.0175.
2. Porter R. W., and Ralston S. H. - Pharmacological management of back pain syndromes, Drugs. **48** (2) (1994) 189-98. https://doi.org/10.2165/00003495-199448020-00006.
3. Mazer M., and Perrone J. - Acetaminophen-induced nephrotoxicity: pathophysiology, clinical manifestations, and management, J. Med. Toxicol **4** (1) (2008) 2-6. https://doi.org/10.1007/BF03160941.
4. Olaleye M. T., and Rocha B. T. - Acetaminophen-induced liver damage in mice: effects of some medicinal plants on the oxidative defense system, Exp. Toxicol. Pathol. **59** (5) (2008) 319-27. https://doi.org/10.1016/j.etp.2007.10.003.
5. Cunha R. R., Ribeiro M. M. A. C., Muñoz R. A. A., and Richter, E. M. - Fast determination of codeine, orphenadrine, promethazine, scopolamine, tramadol, and paracetamol in pharmaceutical formulations by capillary electrophoresis, J. Sep. Sci. **40** (8) (2017) 1815-1823. https://doi.org/10.1002/jssc.201601275.
6. Tsvetkova B., Pencheva I., Zlatkov A., and Peikov P. - Simultaneous high-performance liquid chromatography determination of paracetamol and ascorbic acid in tablet dosage forms, Afr. J. Pharm. Pharmacol. **6** (17) (2012) 1332-1336. https://doi.org/ 10.5897/AJPP12.163.

7. Mallah M. A., Sherazi S. T. H., Bhanger M. I., Mahesar, S. A., and Bajeer M. A. - A rapid Fourier-transform infrared (FTIR) spectroscopic method for direct quantification of paracetamol content in solid pharmaceutical formulations. Spectrochim, Acta - A: Mol. Biomol. Spectrosc **141** (2015) 64-70. https://doi.org/10.1016/j.saa.2015.01.036.
8. Narang J., Malhotra N., Singh S., Singh G., and Pundir C. S. - Monitoring analgesic drug using sensing method based on nanocomposite, RSC Adv. **5** (4) (2015) 2396-2404. https://doi.org/10.1039/C4RA11255E.
9. Li J., Liu J., Tan G., Jiang J., Peng S., Deng M., Qian D., Feng Y., and Liu Y. J. - High-sensitivity paracetamol sensor based on Pd/graphene oxide nanocomposite as an enhanced electrochemical sensing platform, Biosens. Bioelectron **54** (2014) 468-475. https://doi.org/10.1016/j.bios.2013.11.001.
10. Xu Z., Teng H., Song J., Gao F., Ma L., Xu G., Luo X. - A nanocomposite consisting of MnO_2 nanoflowers and the conducting polymer PEDOT for highly sensitive amperometric detection of paracetamol, Mikrochim. Acta **186** (2019) 1-8. https://doi.org/10.1007/s00604-019-3614-3.
11. Kang X., Wang J., Wu H., Liu J., Aksay I. A., and Lin Y. - A graphene-based electrochemical sensor for sensitive detection of paracetamol, Talanta **82** (3) (2010) 754-759. https://doi.org/10.1016/j.talanta.2010.01.009.
12. Qian L., Durairaj S., Prins S., and Chen A. - Nanomaterial-based electrochemical sensors and biosensors for the detection of pharmaceutical compounds, Biosens Bioelectron **175** (2021) 112836. https://doi.org/10.1016/j.bios.2020.112836.
13. dos Santos O. A. L., Sneha M., Devarani T., Bououdina M., Backx B. P., Vijaya J. J., and Bellucci S. - Perovskite/Spinel based graphene derivatives electrochemical and biosensors, J. Electrochem. Soc. **168** (6) (2021) 067506. https://doi.org/10.1149/1945-7111/ac0306.
14. Gonçalves J. M., Rocha D. P., Silva M. N. T., Martins P. R., Nossol E., Angnes L., Rout C. S., and Munoz R. A. A. - Feasible strategies to promote the sensing performances of spinel MCo_2O_4 (M = Ni, Fe, Mn, Cu and Zn) based electrochemical sensors: a review, J. Mater. Chem. C. **9** (25) (2019) 7852-7887. https://doi.org/10.1039/D1TC01550H.
15. Li Y., Chu Y., Li Y., Ma C., and Li L. - A novel electrochemiluminescence biosensor: Inorganic-organic nanocomposite and $ZnCo_2O_4$ as the efficient emitter and accelerator, Sens. Actuators B Chem. **303** (2020) 127222. https://doi.org/10.1016/j.snb.2019.127222.
16. Zhang N., Lu Y., Fan Y., Zhou J., Li X., Adimi S., Liu C., and Ruan S. - Metal–organic framework-derived $ZnO/ZnCo_2O_4$ microspheres modified by catalytic PdO nanoparticles for sub-ppm-level formaldehyde detection, Sens. Actuators B Chem. **315** (2020) 128118. https://doi.org/10.1016/j.snb.2020.128118.
17. Aruchamy K., Balasankar A., Ramasundaram S., and Oh T. H. - Recent Design and Synthesis Strategies for High-Performance Supercapacitors Utilizing $ZnCo_2O_4$-Based, Electrode Materials **16** (15) (2023) 5604. https://doi.org/10.3390/en16155604.
18. Mai Tho N. T., Van Cuong N., Luu Thi V. H., Thang N. Q., and Dang P. H. - A novel n–p heterojunction $Bi_2S_3/ZnCo_2O_4$ photocatalyst for boosting visible-light-driven photocatalytic performance toward indigo carmine, RSC adv. **13** (24) (2023) 16248-16259. https://doi.org/10.1039/D3RA02803H.
19. Zhang J., Cui S., Ding Y., Yang X., Guo K., and Zhao J.-T. - Two-dimensional mesoporous $ZnCo_2O_4$ nanosheets as a novel electrocatalyst for detection of o-nitrophenol

and p-nitrophenol, Biosens. Bioelectron **112** (2018) 177-185. https://doi.org/10.1016/j.bios.2018.03.021.

20. Kim D. S., Moon I. K., Yang J. H., Choi K., Oh J., and Kim S. W. - Mesoporous $ZnCo_2O_4$ nanowire arrays with oxygen vacancies and N-dopants for significant improvement of non-enzymatic glucose detection, J. Electroanal. Chem. **878** (2020) 114585. https://doi.org/10.1016/j.jelechem.2020.114585.
21. Naik K. K., and Rout C. S. - Electrodeposition of $ZnCo_2O_4$ nanoparticles for biosensing applications, RSC adv. **5** (97) (2015) 79397-79404. https://doi.org/10.1039/C5RA11011D.
22. Zhang J., Cui S., Ding Y., Yang X., Guo K., and Zhao J. T. - Two-dimensional mesoporous $ZnCo_2O_4$ nanosheets as a novel electrocatalyst for detection of o-nitrophenol and p-nitrophenol, Biosens. Bioelectron **112** (2018) 177-185. https://doi.org/10.1016/j.bios.2018.03.021.
23. Liu S., Zeng W., and Li Y. - Synthesis of $ZnCo_2O_4$ microrods grown on nickel foam for non-enzymatic glucose sensing, Mater. Lett. **259** (2020) 126820. https://doi.org/10.1016/j.matlet.2019.126820.
24. Xiao X., Wang G., Zhang M., Wang Z., Zhao R., and Wang Y. - Electrochemical performance of mesoporous $ZnCo_2O_4$ nanosheets as an electrode material for supercapacitor, Ionics **24** (2018) 2435-2443. https://doi.org/10.1007/s11581-017-2354-9.
25. Wang W., Chen L., Qi J., Sui Y., He Y., Meng Q., Wei F., and Sun Z. - All-solid-state asymmetric supercapacitor based on N-doped activated carbon derived from polyvinylidene fluoride and $ZnCo_2O_4$ nanosheet arrays, J. Mater. Sci.: Mater. Electron. **29** (2018) 2120-2130. https://doi.org/10.1007/s10854-017-8124-7.
26. Silambarasan M., Ramesh P., Geetha D., Ravikumar K., Ali H. E., Algarni H., Soundhirarajan P., Chandekar K. V., and Shkir M. - A Facile Preparation of Zinc Cobaltite ($ZnCo_2O_4$) Nanostructures for Promising Supercapacitor Applications, J. Inorg. Organomet. Polym. Mater. **31** (2021) 3905-3920. https://doi.org/10.1007/s10904-021-02077-z.
27. Huyen N. N., Tung L. M., Nguyen T. A., Huong Phung T. L., Thang P. D., Vinh N. T., Van Nguyen Q., Oanh Vu T. K., Lam V. D., Le -A. T. - Insights into the Effect of Cation Distribution at Tetrahedral Sites in $ZnCo_2O_4$ Spinel Nanostructures on the Charge Transfer Ability and Electrocatalytic Activity toward Ultrasensitive Detection of Carbaryl Pesticide in Fruit and Vegetable Samples, J. Phys. Chem. C. **127** (25) (2023) 12262-12275. https://doi.org/10.1021/acs.jpcc.3c02039.
28. Liu W., Hu S., Wang Y., Zhang B., Jin R., and Hu L. - Anchoring Plasmonic Ag@AgCl Nanocrystals onto $ZnCo_2O_4$ Microspheres with Enhanced Visible Photocatalytic Activity, Nanoscale Res. Lett. **14** (1) (2019) 108. https://doi.org/10.1186/s11671-019-2922-1.
29. Mater Mahnashi H., Mahmoud A. M., Saad Alkahtani A., and El-Wekil M. M. - Simultaneous electrochemical detection of azithromycin and hydroxychloroquine based on VS_2 QDs embedded N, S @graphene aerogel/cCNTs 3D nanostructure, Microchem J. **163** (2021) 105925. https://doi.org/10.1016/j.microc.2021.105925.
30. Huyen N. N., Dinh N. X., Doan M. Q., Vu N. P., Das R., Le M. T., Thang P. D., and Le A. T. - Unraveling the roles of morphology and steric hindrance on electrochemical analytical performance of α-Fe_2O_3 nanostructures-based nanosensors towards

chloramphenicol antibiotic in shrimp samples, J. Electrochem Soc. **169** (2) (2022) 026507. https://doi.org/10.1149/1945-7111/ac4db0.

31. Nematollahi D., Shayani-Jam H., Alimoradi M., Niroomand S. - Electrochemical oxidation of acetaminophen in aqueous solutions: Kinetic evaluation of hydrolysis, hydroxylation and dimerization processes, Electrochim. Acta **54** (28) (2009) 7407-7415. https://doi.org/10.1016/j.electacta.2009.07.077.
32. Shafiei H., Haqgu M., Nematollahi D., and Gholami M. R. - An experimental and computational study on the rate constant of electrochemically generated N-acetyl-p-quinoneimine with dimethylamine, J. Electrochem Sci. **3** (10) (2008) 1092-1107. https://doi.org/10.1016/S1452-3981(23)15506-4.
33. Nematollahi, D.; Momeni, S.; Khazalpour, S. - A green electrochemical method for the synthesis of acetaminophen derivatives, J. Electrochem Soc. **161** (3) (2013) H75. https://doi.org/10.1149/2.022403jes.
34. Yin T., Li H., Su L., Liu S., Yuan C., Fu D. - The catalytic effect of TiO_2 nanosheets on extracellular electron transfer of Shewanella loihica PV-4, Phys. Chem. Chem. Phys. **18** (43) (2016) 29871-29878. https://doi.org/10.1039/C6CP04509J.
35. Uzun Demet. - Determination of paracetamol based on 3- amino- 4H- 1, 2, 4- triazole coated glassy carbon surface in pharmaceutical sample, Electroanalysis **33** (7) (2021) 1699-1706. https://doi.org/10.1002/elan.202100002.
36. Sadok I., and Tyszczuk-Rotko K. - New, simple and sensitive voltammetric procedure for determination of paracetamol in pharmaceutical formulations, Anal. Chem. Insights **1** (1) (2015). https://doi.org/10.4172/2470-9867.100001.
37. Rodrigues Filho G., Almeida F., Ribeiro S. D., Tormin T. F., Muñoz R. A., Assunção R. M., Barud H. J. D. D., and Pharmacy I. - Controlled release of drugs from cellulose acetate matrices produced from sugarcane bagasse: monitoring by square-wave voltammetry, Drug. Dev. Ind. Pharm. **42** (7) (2016) 1066-1072. https://doi.org/10.3109/03639045.2015.1107093.
38. Noviandri I., and Rakhmana R. - Carbon Paste Electrode Modified with Carbon Nanotubes and Poly(3-Aminophenol) for Voltammetric Determination of Paracetamol, Int. J. Electrochem. Sci. **7** (5) (2012) 4479-4487. https://doi.org/10.1016/S1452-3981(23)19554-
39. Li M., and Jing L. - Electrochemical behavior of acetaminophen and its detection on the PANI–MWCNTs composite modified electrode, Electrochim Acta **52** (9) (2007) 3250-3257. https://doi.org/10.1016/j.electacta.2006.10.001.
40. Narayana P. V., Reddy T. M., Gopal P., and Naidu G. R. - Electrochemical sensing of paracetamol and its simultaneous resolution in the presence of dopamine and folic acid at a multi-walled carbon nanotubes/poly(glycine) composite modified electrode, Anal. Methods **6** (23) (2014) 9459-9468. https://doi.org/10.1039/C4AY02068E.
41. Alothman Z. A., Bukhari N., Wabaidur S. M., and Haider S. - Simultaneous electrochemical determination of dopamine and acetaminophen using multiwall carbon nanotubes modified glassy carbon electrode, Sens. Actuators B: Chem. **146** (1) (2010) 314-320. https://doi.org/10.1016/j.snb.2010.02.024.
42. Tajik S., Sharifi F., Aflatoonian B., and Mohammadi S. Z. - An Efficient Electrochemical Sensor Based on $NiCo_2O_4$ Nanoplates and Ionic Liquid for Determination of Favipiravir

in the Presence of Acetaminophen, Biosens. **13** (8) (2023) 814. https://doi.org/10.3390/bios13080814.

43. Hasanpour F., Taei M., and Tahmasebi S. - Ultra-sensitive electrochemical sensing of acetaminophen and codeine in biological fluids using $CuO/CuFe_2O_4$ nanoparticles as a novel electrocatalyst, J. Food Drug Anal. **26** (2) (2018) 879-886. https://doi.org/10.1016/j.jfda.2017.10.001.
44. Annadurai K., Sudha V., Murugadoss G., and Thangamuthu R. - Electrochemical sensor based on hydrothermally prepared nickel oxide for the determination of 4-acetaminophen in paracetamol tablets and human blood serum samples, J. Alloys Compd. **852** (2021) 156911. https://doi.org/10.1016/j.jallcom.2020.156911.
45. Shahmiri M. R., Bahari A., Karimi-Maleh H., Hosseinzadeh R., and Mirnia N. - Ethynylferrocene–NiO/MWCNT nanocomposite modified carbon paste electrode as a novel voltammetric sensor for simultaneous determination of glutathione and acetaminophen, Sens. Actuators B: Chem. **177** (2013) 70-77. https://doi.org/10.1016/j.snb.2012.10.098.